Journal of Solid State Chemistry **162,** 90–95 (2001)
doi:10.1006/jssc.2001.9359, available online at http://www.idealibrary.com on IDEAL®

$Ln_3T_2N_6$ (Ln = La, Ce, Pr; T = Ta, Nb), a New Family of Ternary Nitrides Isotypic to a High T_c Cuprate Superconductor

Laurent Cario,* Zoltán A. Gál,* Thomas P. Braun,* Francis J. DiSalvo,*
Björn Blaschkowski,† and H.-Jürgen Meyer†

*Baker Laboratory, Department of Chemistry and Chemical Biology, Cornell University, Ithaca, New York 14853-1301; and †Institut für Anorganische Chemie, Universität Tübingen, Auf der Morgenstelle 18 72076 Tübingen, Germany

Received March 13, 2001; in revised form August 3, 2001; accepted August 16, 2001

A new family of ternary nitrides $Ln_3T_{2-x}N_6$ (Ln= rare earth; T= Nb or Ta, $0 \leq x \leq 0.2$) has been successfully synthesized using Ga or Li_3N as a flux. These compounds crystallize in the tetragonal space group *I4/mmm* (No. 139) with parameters $a \approx 4.05$ Å and $c = 20.2$ Å. They are isostructural with the high T_c superconducting cuprate $La_{2-x}Sr_xCaCu_2O_6$. Extended Hückel band structure calculations show that the nitrides contain conducting TN_2 layers similar to the CuO_2 layers. However, magnetic measurements performed on these ternary nitrides do not show any superconducting transition down to 4 K. © 2001 Academic Press

Key Words: **nitrides; transition metals; rare-earth compounds; structure elucidation; superconductors.**

INTRODUCTION

Since the mid-1980s there has been a renewed interest in the chemistry of ternary and quaternary nitrides (1–4). Very often, these new nitrides exhibit novel crystal structures, as well as unexpected and interesting electronic properties. In contrast to the wide variety of ternary nitrides containing group I or II elements in combination with elements of all other groups, the number of nitrides combining rare-earth and transition metals is rather small. The largest family consists of six compounds, M_2TN_3 (M = U, Th, and Ce; T = Cr, Mn), that adopt a defect variant of the well-known K_2NiF_4 structure type (5–7). Ce_2MnN_3 exhibits metallic behavior with metal atoms in unusual oxidation states, namely Ce^{4+} and Mn^{+1}. The three compounds $Ln_3Cr_{10-x}N_{11}$ (Ln = La, Ce, Pr) crystallize in a new cubic structure type and exhibit unusual chromium oxidation states (between +2.4 and +3) (6, 8). The lanthanum phase exhibits metallic behavior with an indication of a superconducting transition around 2 K. In addition, a few other compounds are known: UVN_2, which adopts the $UMoC_2$ structure type (9), $Ln_2Fe_{17}N_3$, which is closely related to the hard magnet Ln_2Fe_{17} (nitrogen atoms are in interstitial positions) (10), and finally $TaThN_3$, which adopts the perovskite structure type (11).

More than half of the known ternary rare earth–transition metal–nitrides adopt structure types derived from perovskite, making it easy to imagine that nitride chemistry can provide compounds with structures related to high T_c superconductors. To this end we have begun an investigation of the ternary systems rare earth–transition metal–nitrogen. Since NbN and TaN have the highest T_c values of binary nitrides, we first focused on the Ln–Nb–N and Ln–Ta–N systems (with Ln = Y, La, Ce, Pr).

EXPERIMENTAL

Synthesis. Two different synthetic routes were used to explore the Ln–Nb–N and Ln–Ta–N systems (with Ln = Y, La, Ce, Pr). Both lead to the same family of new ternary nitrides. The first method is based on the use of Ga as a flux (liquid range 29–2204°C) in which a mixture of the pure metals $Ln:T$:Ga in a 3:2:9 ratio were heated in a RF furnace at 1600°C, first under Ar for 12 h then under N_2 for 2 days. These reactions yielded a mixture of binary nitrides and black metallic crystals. The other method uses Li_3N as a flux and as reactive nitrogen source. Mixtures of $Ln:T:Li_3N$ in 3:2:10 molar ratios were weighed under an Ar atmosphere and then arc-welded in tantalum or niobium ampoules. These ampoules were then sealed in silica tubes and heated at 1030°C for 60 h. After cooling down, the metal ampoules contained a metallic matrix of Li in which black crystals were embedded. After dissolving the Li matrix in water, pure air and moisture stable crystals of the ternary nitrides were obtained.

Analysis. Microprobe analysis on crystals from batches containing La/Ta, La/Nb, and Ce/Ta revealed a rare earth-to-transition metal ratio of 3:2. A phase with the same composition could not be found in the Ce/Nb,

0022-4596/01 $35.00

Y/Nb, and Y/Ta reaction mixtures. In one batch of La/Ta that contained an excess of lanthanum, some of the analyzed crystals revealed a higher rare earth-to-transition metal ratio $3/(2-x)$ ($0 < x < 0.2$), suggesting the possibility of nonstoichiometry for the transition metal. Finally, the microprobe analysis ascertained the presence of nitrogen in these compounds while no oxygen was detected.

Magnetic measurements. Magnetic measurements were carried out on a SQUID magnetometer (quantum design) for the tantalum and niobium phases. Samples of 40–60 mg were weighed in gelatin capsules and measured in DC mode with fields between 10 and 2000 Oe.

Crystal structure analysis. Black metallic truncated parallelepiped crystals suitable for X-ray structure analysis were chosen from the different batches. The intensities were collected on a Bruker Smart CCD (ω-scan) equipped with a graphite monochromator and using Mo$K\alpha$ ($\lambda = 71.073$ pm) radiation. All data sets are consistent with a tetragonal symmetry ($a \approx 4.05$ Å and $c \approx 20.2$ Å) and the space group $I4/mmm$ (No. 139). The intensity of the different data sets were corrected for Lorentz polarization and subsequently corrected for absorption via a Gaussian analytical method (the crystal shape and dimensions were previously optimized with the Stoe X-shape program (1996) on the basis of equivalent reflections). All data treatments were carried out with the SHELXTL-5.03 program package (structure solution, direct method; structure refinement, full-matrix least squares based on $|F^2|$). Single-crystal and powder X-ray analysis revealed that the new nitrides have the compositions $La_3Ta_2N_6$, $La_3Ta_{1.80}N_6$, $Ce_3Ta_{1.97}N_6$, and $La_3Nb_2N_6$. The refinement of the site occupancy factor of the transition metal led in some cases to a significant decrease of the reliability factor. No residue on the electronic density map was seen on the 2b site $(0, 0, \frac{1}{2})$ while the presence of nitrogen or oxygen on this site would lead to an octahedral environment for the transition metal atom. Attempts to refine oxygen or nitrogen on this site lead to meaningless values of the thermal displacement parameters even if the site is partially occupied. Refining the structure with oxygen instead of nitrogen on both 4e sites increases the reliability factors and the thermal displacement parameters. These results are in agreement with the microprobe analysis and show that these compounds are not oxynitrides. Thus the general formula for this new family of nitrides is $Ln_3T_{2-x}N_6$ with $0 \leq x \leq 0.2$. The cell parameters and other details concerning the X-ray data collection and structural refinement for each compound are gathered in Table 1 (12). Table 2 gives the atomic coordinates for the different compounds and Table 3 the main bond distances for $Ln_3T_2N_6$ (Ln = La, Ce; T = Nb, Ta). A powder diffraction pattern performed on $Pr_3Ta_2N_6$ showed that this compound is isotypic with the former nitride (13).

TABLE 1
Crystallographic Data and Refinement Results for $La_3Ta_2N_6$, $La_3Ta_{1.80}N_6$, $Ce_3Ta_{1.97}N_6$, and $La_3Nb_2N_6$

Empirical formula	$La_3Ta_2N_6$	$La_3Ta_{1.80}N_6$	$Ce_3Ta_{1.97}N_6$	$La_3Nb_2N_6$
Formula weight	862.69	826.50	860.89	686.61
Temperature (K)	293(2)	155(2)	155(2)	155(5)
Unit cell dimensions (Å)	$a = 4.0674(2)$	$a = 4.0399(6)$	$a = 4.0451(8)$	$a = 4.0698(5)$
	$b = 4.0674(2)$	$b = 4.0399(6)$	$b = 4.0451(8)$	$b = 4.0698(5)$
	$c = 20.451(1)$	$c = 20.185(4)$	$c = 19.995(4)$	$c = 20.154(3)$
Volume (Å^3)	338.33(3)	329.44(10)	327.18(13)	333.81(8)
Z	2	2	2	2
Density (calculated) (Mg/m^3)	8.468	8.332	8.739	6.831
Absorption coefficient (mm^{-1})	50.671	48.736	53.183	22.035
$F(000)$	718	689	720	590
θ range	1.99° to 27.23°	2.02° to 27.87°	2.04° to 27.71°	2.02° to 27.68°
Reflections collected	1052	873	855	1202
Independent reflections	151	147	143	153
Absorption correction	Analytical	Analytical	Analytical	Analytical
Crystal dim. (mm^3)	$0.06 \times 0.05 \times 0.04$	$0.07 \times 0.04 \times 0.02$	$0.07 \times 0.02 \times 0.02$	$0.05 \times 0.05 \times 0.02$
R(int)	0.0643	0.0601	0.0517	0.0539
Max./min transmission	0.2320/0.1081	0.4437/0.1335	0.4304/0.1254	0.6622/0.3119
Data/restraints/param.	151/0/14	147/0/15	143/0/15	153/0/14
R_1/wR_2 All	0.0395/0.0653	0.0341/0.0671	0.0264/0.0454	0.0211/0.0373
$[I > 2\,\sigma(I)]$	0.0364/0.0640	0.0243/0.0506	0.0233/0.0444	0.0204/0.0372
Largest diff. peak/hole (e.Å^{-3})	1.540/−2.860	1.552/−2.893	2.159/−2.179	1.048/−1.509

TABLE 2
Fractional Atomic Coordinates and Isotropic (or Equivalent) Atomic Displacement Parameters for $La_3Ta_2N_6$, $La_3Ta_{1.80}N_6$, $Ce_3Ta_{1.97}N_6$, and $La_3Nb_2N_6$

		$La_3Ta_2N_6$		$La_3Ta_{1.8}N_6$[a]		$Ce_3Ta_{1.97}N_6$[a]		$La_3Nb_2N_6$	
Atom	site	Z	U_{iso}/U_{eq}	Z	U_{iso}/U_{eq}	Z	U_{iso}/U_{eq}	Z	U_{iso}/U_{eq}
T_1	4e	0.39941(6)	0.0041(5)	0.39934(7)	0.0023(6)	0.39969(4)	0.0019(4)	0.39895(5)	0.0035(3)
Ln_1	2a	0	0.0061(6)	0	0.0043(7)	0	0.0028(5)	0	0.0032(3)
Ln_2	4e	0.81779(9)	0.0074(9)	0.81957(9)	0.0054(7)	0.81853(6)	0.0047(5)	0.82019(3)	0.0043(3)
N_1	4e	0.3034(14)	0.016(7)	0.3030(13)	0.011(6)	0.3021(10)	0.018(5)	0.3019(5)	0.012(2)
N_2	4e	0.4132(9)	0.015(4)	0.4132(9)	0.008(4)	0.4153(6)	0.012(3)	0.4153(3)	0.0069(13)

[a]Site occupancy factors for the Ta:0.885(9) in $La_3Ta_{1.8}N_6$ and 0.984(6) in $Ce_3Ta_{1.97}N_6$

RESULT AND DISCUSSION

These compounds are isostructural with the double-layer superconducting copper oxides $La_{2-x}Sr_xCaCu_2O_6$, which exhibit T_c values up to 60 K, and with the nonmetallic cobalt compound $Sr_2Ln_{0.8}Ca_{0.2}Co_2O_6$ (14, 15). Figure 1 gives a perspective view of the structure. The transition metal (Wyckoff site 4e, $z = 0.40$) is located slightly above the basal plane of a nitrogen square pyramid. The square pyramids form extended 2D layers via corner sharing. According to the lower coordination number of the transition metal in the title compounds (5) than in the binary compounds (6), the T–N bond distances (T = Nb or Ta) within the square pyramids (see Table 3) are slightly shorter than what is reported for the TN binary compounds (Nb–N, 2.19 Å; Ta–N, 2.16 Å). The rare-earth atoms (site 4e, $z = 0.82$) together with the apical nitrogen of the square pyramid (site 4e, $z = 0.30$) form a two-dimensional rock salt layer. As shown in Table 3 the rare earth–nitrogen bond distances found in $Ln_3T_2N_6$ (Ln = La, Ce; T = Nb, Ta) are comparable to the distances found in LaN (2.65 Å) and CeN (2.60 Å).

TABLE 3
Main Bond Distances for $La_3Ta_2N_6$, $La_3Ta_{1.80}N_6$, $Ce_3Ta_{1.97}N_6$, and $La_3Nb_2N_6$

	$La_3Ta_2N_6$	$La_3Ta_{1.80}N_6$	$Ce_3Ta_{1.97}N_6$	$La_3Nb_2N_6$
	Main transition metal–nitrogen distance (Å)			
T_1–N_1 apical × 1	1.96(3)	1.94(3)	1.951(19)	1.955(10)
T_1–N_2 square × 4	2.053(3)	2.039(3)	2.0465(19)	2.0615(10)
	Main rare earth–nitrogen distances (Å)			
Ln_1–N_2 × 8	2.699(12)	2.674(12)	2.638(8)	2.656(4)
Ln_2–N_1 × 1	2.48(3)	2.47(3)	2.413(19)	2.461(10)
Ln_2–N_1 × 4	2.891(3)	2.876(3)	2.879(2)	2.9012(13)
Ln_2–N_2 × 4	2.818(13)	2.767(12)	2.799(9)	2.796(4)

A general description for the new nitrides as well as the superconducting cuprates is based on the Ruddlesden–Popper layering scheme for the perovskite-related oxo-titanates $(SrTiO_3)_n(SrO)$ (16). They are built up from n infinite perovskite-like layers alternating with one SrO rock salt layer. The new nitrido-metallates (and corresponding oxo-cuprates) contain perovskite-like double layers ($n = 2$), where, in contrast to the oxo-titanates, one nitrogen (posi-

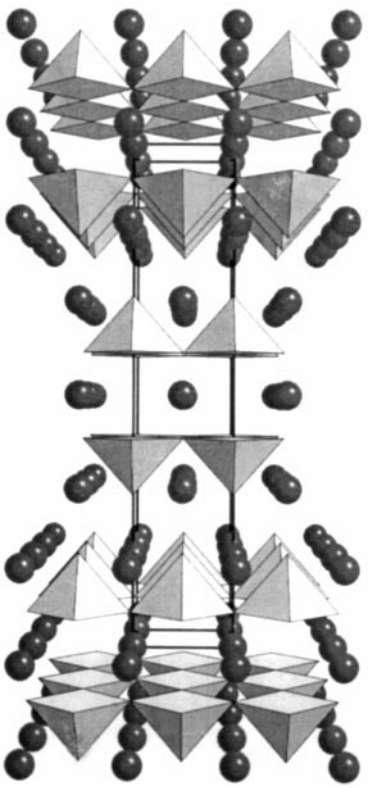

FIG. 1. Structure of $Ln_3T_{2-x}N_6$ shown in perspective along the a axis. The layers of corner-sharing square pyramids are separated by rare-earth atoms displayed as black spheres.

TABLE 4
Slater-Type Orbital Energies and Exponents

Orbital	H_{ii}, eV	ξ_1	c_1	ξ_2	c_2
N					
2*s*	−26.223	1.885			
2*p*	−13.841	1.728			
La					
6*s*	−4.637	1.318			
6*p*	−3.233	1.142			
5*d*	−7.316	3.153	0.594	1.338	0.612
Nb					
5*s*	−5.923	1.403			
5*p*	−3.757	1.186			
4*d*	−10.001	2.995	0.6859	1.333	0.4619
Ta					
6*s*	−5.979	1.658			
6*p*	−3.757	1.417			
5*d*	−9.569	3.478	0.6739	1.606	0.4959

tion (site 2b:$0,0,\frac{1}{2}$) remains vacant. Also the above-mentioned family of ternary nitrides M_2TN_3 with defect K_2NiF_4 structure type as well as $TaThN_3$ could be viewed in terms of the Ruddlesden–Popper scheme with $n = 1$ and $n = \infty$, respectively.

The structural similarity to the superconducting oxocuprates suggests an examination of their electronic structures. We examined the chemical bonding in $La_3T_2N_6$ by means of the extended Hückel method (17, 18). The basis set consisted of Slater-type atomic orbitals with energies and exponents gathered in Table 4. The 3D band structure calculations have been calculated in the (small) primitive cell containing one formula unit (11 atoms/69 orbitals) at the special points $\Gamma(0,0,0)$, $X(0,0,\frac{1}{2})$, $P(\frac{1}{4},\frac{1}{4},\frac{1}{4})$, $N(0,\frac{1}{2},0)$, and $Z(\frac{1}{2},\frac{1}{2},-\frac{1}{2})$ and for 100 points along each symmetry line connecting these. The DOS has been calculated by averaging over 150 K points. The density of states (DOS) and the band structure of $La_3Nb_2N_6$ are shown in Fig. 2. It confirms the expected distribution of states with fully occupied *s* and *p* bands of N. The La *d* band lies above the Fermi level (i.e., La^{3+}) that cuts through the bottom of the Nb *d* band, predicting metallic behavior (i.e., formally $Nb^{4.5+}$). As expected, there is a significant mixing of the N 2*p* orbitals with the Nb 4*d* states and to a smaller extent with the La 5*d* orbitals. In the band structure (depicted on the left in Fig. 2) little dispersion is found along k_z and hence the electronic structure can be described as quasi-two dimensional. A calculation for a single $\infty^2[NbN_{4/2}N]$ layer reproduces the corresponding bands and DOS for the 3D system very well. Therefore, the important features of the band structure of $La_3Nb_2N_6$, especially around the Fermi level, are determined by the nitrogen–niobium interactions within the $\infty^2[NbN_{4/2}N]$ layer. Like the superconducting cuprates, $La_3Nb_2N_6$ can be described as a stacking of charge reservoir and acceptor layers. Due to the particular geometry of the NbN_5 square pyramid (the niobium distance to the apical nitrogen (1.95 Å) is shorter than the distance to the nitrogens of the basal plane (2.06 Å)), the antibonding π interaction between the N 2*p* and the Nb 4*d* orbitals is enhanced along *z*. Therefore the "t_{2g} orbitals" are split by π^* interactions so that the d_{xy} orbital (b_2) lies slightly below the e set (d_{xz}, d_{yz}). The band order ($d_{xy}, d_{xz}/d_{yx}, d_z^2, d_{x_2-y_2}$) of the molecular orbital diagram is preserved in the extended system, but the energy differences are more pronounced due to the interactions with neighboring cells, and the picture is complicated furthermore by a number of avoided crossings.

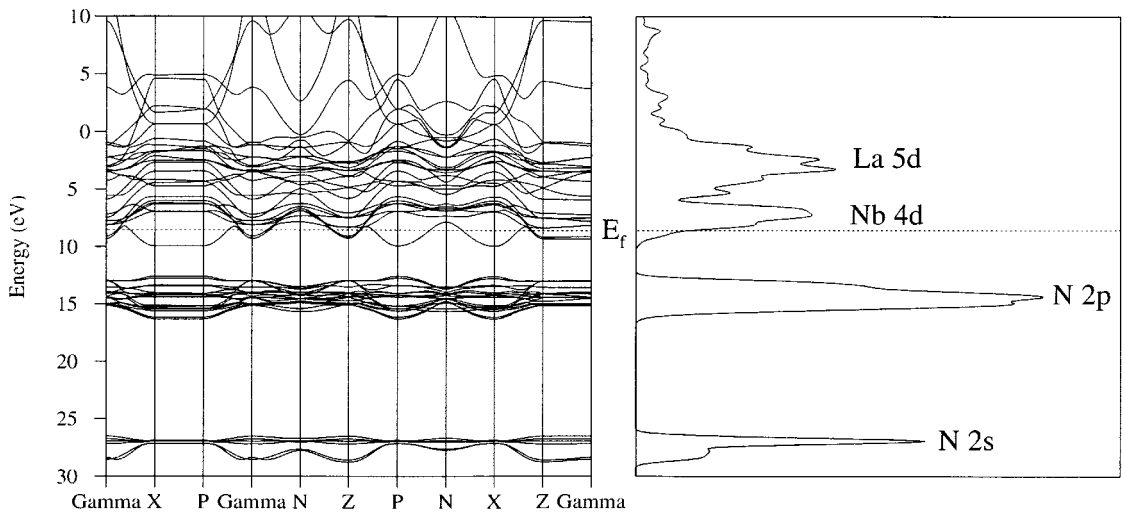

FIG. 2. Density of states (DOS) and band structure of $Ln_3Nb_2N_6$ as obtained from the extended Hückel method. The main character of each band is indicated.

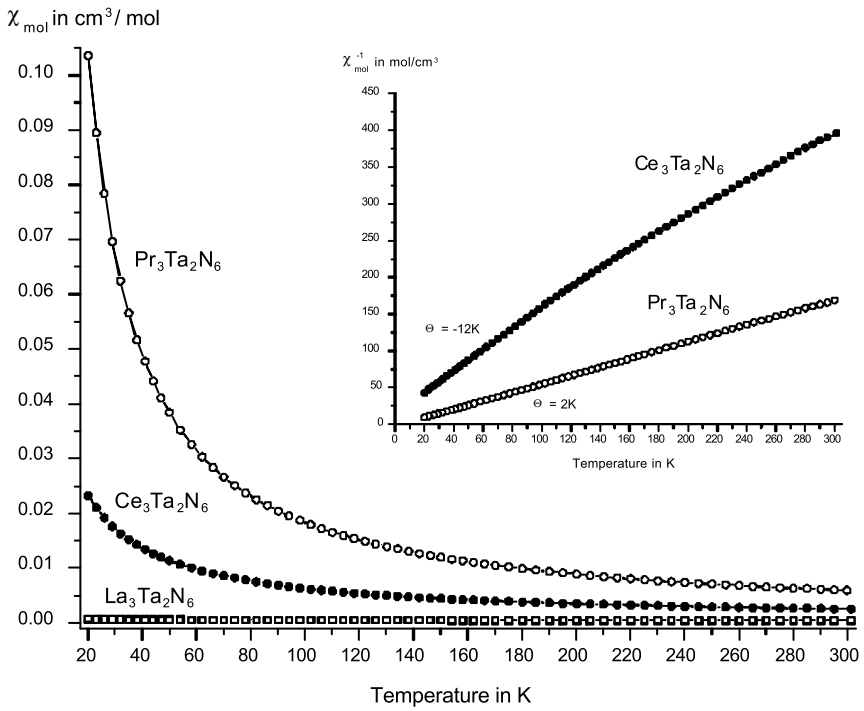

FIG. 3. Magnetic susceptibilities for samples of $La_3Ta_2N_6$, $Ce_3Ta_2N_6$, and $Pr_3Ta_2N_6$. $La_3Ta_2N_6$ exhibits Pauli paramagnetism, while $Ce_3Ta_2N_6$ and $Pr_3Ta_2N_6$ follow a Curie–Weiss law as shown in the inset.

However, the Fermi level cuts only through the d_{xy} band, which is partially filled. This allows us to discuss the electronic properties of $La_3Nb_2N_6$ in a simple one-band electron-doped model.

Both the nitrido-metallate and the oxo-cuprate families contain isostructural conducting $\infty^2[NbN_{4/2}N]$ and $\infty^2[CuO_{4/2}O]$ layers. However, in the oxo-cuprates the states at the Fermi level are hybrids of Cu $3d_{x_2-y_2}$ and O $2p_x/p_y$ (σ^* bands), while in the nitrido-metallates the states at the Fermi level are hybrids of the nitrogen p orbitals and the metal d_{xy} orbitals (π^* bands). In addition, for the oxo-cuprates the highest occupied bands have a strong O $2p$ character ($\approx 50\%$), while in the nitrido-metallates these bands are mostly of metal d character (N admixture $\approx 10\%$). Another important difference must be pointed out. In the oxo-cuprates high T_c values are found close to the metal–insulator transition. This suggests that electronic correlations play an important role in their superconductivity. Since the early transition metal $4d$ and $5d$ orbitals are more diffuse than the Cu $3d$ orbitals, broader bands result, leading to a diminished importance of the electronic correlations in the nitrido-metallates.

Despite the different bonding situations, the structural similarities of the high T_c superconducting oxo-cuprates with these nitrido-metallates prompted us to investigate their physical properties. Magnetic measurements of the tantalum-containing nitrides $La_3Ta_2N_6$, $Ce_3Ta_2N_6$, and $Pr_3Ta_2N_6$ in the range of 20–300 K revealed temperature-independent Pauli paramagnetism for the lanthanum compound and Curie–Weiss behavior for the cerium and praseodymium compound. The linear dependence of $1/\chi$ on T (Curie–Weiss law) for the cerium and praseodymium compound is shown in the inset of Fig. 3. Small values obtained for θ (-12 K and 2 K) indicate small exchange interactions between the respective magnetic ions. Calculated magnetic moments (2.5 μ_B for the Ce compound, 3.75 μ_B for the Pr compound) are in good agreement with the theoretical values for trivalent rare-earth metals (2.54 μ_B for Ce^{3+} and 3.58 μ_B for Pr^{3+}). These results are consistent with our band structure calculations, considering a trivalent oxidation state for the rare-earth ions. Pauli paramagnetic behavior for the lanthanum compound is due to partially occupied d bands of the transition metal. This temperature-independent behavior, also expected to be present in compounds containing magnetic rare-earth ions, is masked by their strong f-magnetism. In the case of $La_3Nb_2N_6$ we measured the magnetization of a sample down to 2 K in a magnetic field of 10 Oe. At high temperatures the expected Pauli paramagnetism is observed, but below 4 K a transition to a diamagnetic state is observed that can likely be assigned to a metal–superconductor transition (20% in volume). However, not all the different samples of

$La_3Nb_2N_6$ show this transition, suggesting that small differences in stoichiometry of $La_3Nb_{2-x}N_6$ affect T_c or that a superconducting impurity is sometimes present. The other members of the $Ln_3T_2N_6$ family do not show a superconducting transition down to 3 K.

The nitrido-metallates and the oxo-cuprates, while containing isostructural conducting layers, exhibit very different electronic behavior. This observation is in agreement with other measurements on perovskite oxides containing d^1 transition metals. $LaTiO_3$, for example, is a Mott insulator that becomes metallic at a low level of substitution of La by Sr, but it is never superconducting above 4 K (19). This suggests that the microscopic mechanism for high T_c superconductivity is more related to the unusual electronic situation prevalent in the cuprates rather than to their structural features. However, the exploration of ternary and quaternary transition metal nitrides is still in its infancy. We hope that future research may lead to nitride compounds that fulfill requirements for high T_c superconductivity.

ACKNOWLEDGMENTS

We thank Dr. E. Lobkovsky (single-crystal diffraction) and Mr. J. Hunt (SEM microprobe) for the use of their facilities here at Cornell University. The SEM microprobe is one of the Cornell Center for Materials Research Shared Experimental Facilities, supported through the National Science Foundation Materials Research Science and Engineering Centers program (DMR-0079992). Financial support by the NEDO foundation is gratefully acknowledged. The French foreigner office is thanked for providing to L.C. a LAVOISIER Grant. We also thank the Deutsche Forschungsgemeinschaft for financial support of this work.

REFERENCES

1. N. E. Brese and M. O'Keeffe, *Struct. Bonding* (Berlin) **79,** 309–378 (1992).
2. S. Kikkawa, H. Sugiyama, T. Ohmura, F. Kanamarui, T. Hinomura, and S. Nasu, *Chem. Trans. Met. Carbides Nitrides* 175–190 (1996).
3. R. Marchand, *Handb. Phys. Chem. Rare Earths* **25,** 51–99 (1998).
4. R. Niewa and F. J. DiSalvo, *Chem. Mater.* **10,** 2733–2752 (1998).
5. R. Benz and W. H. Zachariansen, *J. Nucl. Mater.* **37,** 109–113 (1970).
6. S. Broll and W. Jeitschko, *Z. Naturforsch. B* **50,** 905–912 (1995).
7. R. Niewa, G. Vajenine, F. J. DiSalvo, H. Luo, and W. B. Yelon, *Z. Naturforsch. B* **53,** 63–74 (1998).
8. R. Marchand and V. Lemarchand, *J. Less-Common Met.* **80,** 157–63 (1981).
9. K. E. Spear and J. M. Leitnaker, *High Temp. Sci.* **3,** 29–40 (1971).
10. O. Isnard, S. Miraglia, J. L. Soubeyroux, and D. Fruchart, *J. Alloys Compd.* **190,** 129–135 (1992).
11. N. E. Brese and F. J. DiSalvo, *J. Solid State Chem.* **120,** 378–380 (1995).
12. Further details of the crystal structure investigations may be obtained from the Fachinformationszentrum Karlsruhe, D-76344 Eggenstein-Leopoldshafen, Germany, on quoting the depository numbers CSD-411471 ($La_3Ta_2N_6$), CSD-411472 ($La_3Ta_{1.80}N_6$), CSD-411474 ($Ce_3Ta_{1.97}N_6$), and CSD-411473 ($La_3Nb_2N_6$).
13. For $Pr_3Ta_2N_6$ Powder diffraction experiments were carried out on a STADI-P powder diffractometer (Stoe) in transmission mode equipped with a germanium monochromator using Cu$K\alpha$ radiation (λ = 154.058 pm). Diffraction data were collected in the range 8°–94° 2θ. All 28 reflections (with $I > 0.03I_{max}$.) were indexed in a tetragonal I unit cell with a = 403.61(3) pm and c = 1971.27(13) pm.
14. R. J. Cava, B. Batlogg, R. B. Van Dover, J. J. Krajewski, J. V. Waszczak, R. M. Fleming, W. F. Peck, Jr., L. W. Rupp, Jr., P. Marsh, A. C. W. P. James, and L. F. Schneemeyer, *Nature* (*London*) **345,** 602–604 (1990).
15. K. Yamaura, Q. Huang, and R. J. Cava, *J. Solid State Chem.* **146,** 277–286 (1999).
16. S. N. Ruddlesden and P. Popper, *Acta. Crystallogr.* **11,** 54–55 (1958).
17. (a) R. Hoffmann, *J. Chem. Phys.* **39,** 1397–1412 (1963); (b) R. Hoffmann and W. N. Lipscomb, *J. Chem. Phys.* **36,** 2179–2189 (1962).
18. Extended Hückel molecular orbital and band structure calculations have been performed with the YAeHMOP package (G. A. Landrum and W. V. Glassey, *bind* 3.0; G. A. Landrum, *viewkel* 3.0).
19. Y. Tokura, Y. Taguchi, Y. Okada, Y. Fujishima, T. Arima, K. Kumagai, and Y. Iye, *Phys. Rev. Lett.* **70,** 2126 (1993).